WP1200

Preliminary analyses of ET algorithms

Prepared by:

Diego Miralles

University of Bristol, UK

Matthew McCabe

KAUST, Saudi Arabia

Carlos Jiménez

Estellus, France

Table of Contents

1 – Rationale

In situ measurements usually provide a rather accurate estimate of land-surface evaporation (*ET*) in a given point in space and time. However, there is a necessity to routinely obtain *ET* estimates over large areas for agricultural, hydrological and climatological studies. Due to the reduced area sampled by ground observations, the applicability of satellite remote sensing to retrieve *ET* has been explored over the last couple of decades. However, neither *ET* nor any of its components can be directly sensed from satellites, as heat fluxes do not absorb nor emit electromagnetic signals directly. Nonetheless, the last three decades have seen substantial progress in the combined field of evaporation and remote sensing.

Current methodologies concentrate on the derivation of *ET* by combining some of the satellite-observable physical variables that are linked to the evaporation process. Some of the existing algorithms differ in their purpose of application, which to a certain extent defines the type of remote sensing data used and the amount of required ancillary data. The majority use some form of thermal and visible data, with only a few applying microwave observations. Some of these methodologies are fully empirical, others are based on more physically-based calculations of *ET* via formulations like the ones of [*Monteith*, 1965] and [*Priestley and Taylor*, 1972], or focus on solving the surface energy balance targeting the accurate determination of the sensible heat flux (*H*). Most of the early methods were designed for local-scale studies and agricultural and water management practices, while more recent methodologies have started to pursue the coverage of the entire globe. The joint development of satellite sensors and computing science allows the continuous improvement of these algorithms and the development of new ones.

This project aims to advance the improvement and characterization of *ET* estimates from satellite observations, both at continental and regional scales. A cross-comparison, error assessment, and validation exercise of a selection of state-of-art algorithms will be undertaken at different spatial domains and resolutions. The present document explores the advantages and limitations of a suite of currently existing algorithms with the aim of selecting a subset of appropriate methods for future project activities. In Sect. 2 and 3 we will explore the requirements of current algorithms and assess their applicability at regional and continental scale. Based on this assessment, a pre-selection of the best-suited algorithms will be presented in Sect. 4.

The following classifications aim to provide an overview of the most relevant *ET* methods designed for satellite observations. Note that the categories are not exclusive and do not compile all the existing efforts. The classifications are exclusively dedicated to satellite observation-based methodologies specifically designed to derive *ET* with low requirements of

	Institution	Q_{le}	Q_h	R_n	Resolution
		Satellite-Based Products			
UCB	University of California Berkeley	Physical-biological, Priestley-Taylor, inputs from ISLSCP-II (SRB, CRU, AVHRR)	$R_n - Q_{le}$	SRB	1986–95 monthly 1° × 1°
UMD	University of Maryland	Empirical (regression, AmeriFlux Q_{le}), inputs from ISLSCP-II (SRB, CRU, AVHRR)	$R_n - Q_{le}$	SRB	1986–95 monthly 1° × 1°
PRU	Princeton University	Penman-Monteith, inputs from ISCCP, AVHRR, NCEP/NCAR	$R_n - Q_{le}$	ISCCP-FD	1986–06 daily 2.5° × 2.5°
PAO	Paris Observatory	Empirical (neural networks, GSWP modeled Q_{le}), inputs from ISCCP, ERS, SSMI, AVHRR		$Q_{le} + Q_h$	1992–99 monthly 1/4° × 1/4°
MPI	MPI for Biogeochemistry	Empirical (tree ensemble, FluxNet measured Q_{le}) inputs from CRU, GPCC, AVHRR		$Q_{le} + Q_h$	1982–08 monthly 1/2° × 1/2°
		Reanalysis			
MER	NASA-GMAO	MERRA reanalysis, GEOS-5 atmospheric model coupled with Catchment land model			1979– 1-hourly 1/2° × 2/3°
NCE	NCEP/NCAR	NCEP-DOE reanalysis, atmospheric model coupled with OSU land model			1979– 6-hourly 2.5° × 2.5°
ERA	ECMWF	ERA Interim reanalysis, atmospheric model coupled with TESSEL land model			1989–98 6-hourly 3/4° × 3/4°
		Off-Line Land Surface Models			
GSW	GLASS/ISLSCP	Multi-model ensemble, off-line forced with ISLSCP-II		SRB	1986–95 monthly 1° × 1°
NOA	NCAR/OSU/AFWA/HL	Equally off-line forced participating models driven by GLDAS		1993 ERA15 1994/5 NCEP/R1	1979– 3-hourly 1° × 1°
CLM	NCAR +			SRB-bias corrected	
MOS	NASA-GSFC				

Table 1 – Summary of surface fluxes compared in [Jimenez et al., 2011].

ancillary data. More general reviews of these methodologies can be found in [*Courault et al.*, 2005], [*Kalma et al.*, 2008] and [*Wang and Dickinson*, 2012]. Notice also that other methodologies based on relatively complex land surface models are also producing global *ET* estimates for climatological applications. The land surface models can be coupled with an atmospheric model that assimilates observational data, or can be forced off-line by observational or model data, and they are constructed to provide a complete characterization of surface energy and water budget processes (and not just to estimate *ET*). In the framework of the Global Energy and Water Cycle Experiment (GEWEX) Data Assimilation Panel (GDAP) LandFlux-Eval initiative, the first satellite-based *ET* products (reported as latent heat fluxes) and these other estimates have been inter-compared [*Jimenez et al.*, 2011; Mueller et al., 2011]. To give an idea of the type of *ET* products analysed, and the differences found, Table 1 and Figure 1 are reprinted from [*Jimenez et al.*, 2011]. For the rest of the document, only the project-objective satellite-based methodologies are discussed.

2 – Algorithms reported for local and regional scales

2.1 – Simplified Method

The Simplified Method was originally designed to derive *ET* from aerial observations in the visible and infrared part of the spectrum. The method calculates daily *ET* as a direct function of daily net radiation (R_n) and inverse function of the difference between instantaneous midday observations of air temperature (T_a) and surface temperature (T_s). The original formula was derived at field-scale by [*Jackson et al.*, 1977], and later analyzed by [*Seguin and Itier*, 1983]. The calculation of daily *ET* is done via:

$$ET = R_n - b\ (T_s - T_a)^n \quad (1)$$

where *b* and *n* are constants that require local calibration. This equation is essentially a semi-empirical approximation to the surface energy balance equation, which relates the partitioning of R_n in latent (λET), sensible (*H*) and ground (*G*) heat fluxes:

$$R_n = \lambda ET + H + G \quad (2)$$

where λ is the latent heat of vaporization, and therefore the latent heat flux (λET) is nothing but the energy spent in evaporating a given volume (i.e. *ET*) of water. Different studies have analysed the applicability of this method and the validity of its assumptions (e.g. [*Seguin and Itier*, 1983]). Some studies have incorporated empirical parameterizations of *b* and *n* based on windspeed, surface roughness, *NDVI* (Normalized Difference Vegetation Index) or atmospheric stability (e.g. [*Carlson and Buffum*, 1989]). Additionally, [*Carlson et al.*, 1990] propose a modification of this method to estimate root-zone soil moisture, surface soil moisture and vegetation fraction targeting the monitoring of crop water requirements. This modification uses *NDVI* and T_s in combination with a transfer model.

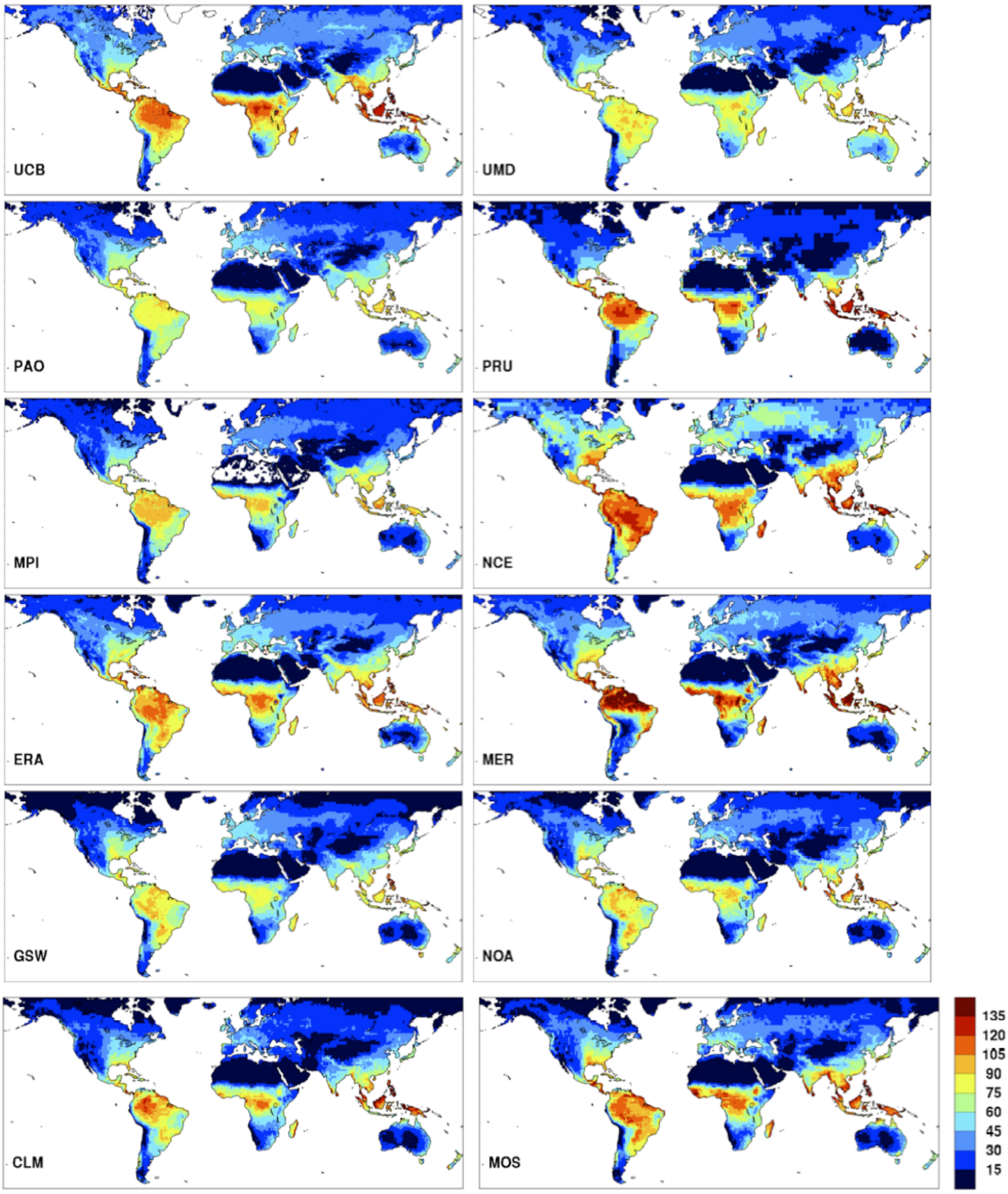

Figure 1 – The 1994 yearly averaged surface latent heat fluxes from the products described in Table 1 [*Jimenez et al.*, 2011].

Advantages

- A priori it can be operational from local to regional scale.
- Relatively simple formulation with low data requirements. The radiative fluxes at the surface cannot be directly measured, but they can be inferred by radiation algorithms

combining measured radiances at the top of the atmosphere and meteorological inputs from satellite measurements and other sources, like those from the GEWEX Surface Radiation Balance (SRB, [*Stackhouse et al.*, 2004]) or International Satellite Cloud Climatology Project (ISCCP) ([*Zhang et al.*, 2004]). Instantaneous temperature observations may be obtained from thermal infrared data using geostationary satellite sensors during midday.

Limitations

- The method implies a constant ratio between H and R_n and a negligible G.
- It relies on optical and thermal instantaneous observations and therefore only works under clear-sky conditions.
- The need for midday temperatures implies a requirement of data from geostationary satellites, which complicates continental to global-scale applications.
- It requires local calibration (of b and n) that complicates the use at continental scale.
- Up to date it has not been applied to create a continuous large-scale dataset of ET.

2.2 – Within-Image Variability Approaches

[*Goward et al.*, 1985], [*Nemani and Running*, 1989] and [*Price*, 1990] first proposed the use of the spatial correlation between T_s and *NDVI* to derive evaporative stress. The rationale is that, due to evaporative cooling, the spatial distribution of satellite-observed temperature and vegetation cover should be negatively correlated. The slope of this relation between T_s and *NDVI* at a particular pixel can be used as a proxy for the evaporative stress and the soil moisture status in that pixel. This technique was later known as the Triangle Method and progressed substantially over the next decades ([*Carlson et al.*, 1995]; [*Carlson*, 2007]). However, estimates of evaporative stress still require an estimate of potential evaporation (ET_p) to be translated into ET. [*Jiang and Islam*, 2001] or [*Batra et al.*, 2006] elaborated on the combination of the Triangle Method and ET_p estimates via the Priestley and Taylor (PT) equation (see Sect. 3.3). Others like [*Schüttemeyer et al.*, 2007] have proposed the use of the [*Makkink*, 1957] equation to compute ET_p. The Triangle Method is used for agricultural applications; in this sense, its rationale can be visualized in a simple way: areas with disproportionally high T_s suggest water shortage and hence the need for irrigation.

A somehow different approach is the Simplified Surface Energy Balance Index (S-SEBI) by [*Roerink et al.*, 2000], which follows from earlier work by [*Menenti and Choudhury*, 1993]. Using a cloud-free thermal or near visible image, S-SEBI derives the evaporative fraction by plotting the spatial variability of T_s against the surface albedo (instead of *NDVI*). This evaporative fraction is then multiplied by the available energy ($R_n - G$) to derive λET. S-SEBI requires reasonably constant atmospheric conditions across the image. It has however already been applied over the entire Iberian Peninsula by [*Sobrino et al.*, 2007] using 1 km resolution Advanced Very High Resolution Radiometer (AVHRR) data.

Arguably the most sophisticated algorithm in this category is the Surface Energy Balance Algorithm for Land (SEBAL) detailed in [*Bastiaanssen et al.*, 1998] which solves the energy balance (eq. 2) and calculates ET as the residual.

While the term G is often less problematic (see below), the computation of H is complicated and usually involves calculation via the electrical analogue from:

$$H = \rho c_p \frac{\Delta T_a}{r_a} \tag{3}$$

where ρ is the air density, c_p the specific heat of air at constant pressure and ΔT_a refers to the gradient of air temperature between the surface and a reference level. The term r_a is the aerodynamic resistance to sensible heat transfer between the two levels in which T_a is considered. To acknowledge that the T_s observed by satellite sensors is not the aerodynamic temperature at surface level required in eq. (3), [*Bastiaanssen et al.*, 1998] propose to empirically derive ΔT_a based on the within-image variability of T_s. SEBAL requires data of T_s, radiation and $NDVI$; the latter is used to estimate G and also as a proxy of the surface roughness in the derivation of r_a.

There have been several applications of SEBAL at the local to regional scales, especially directed to the field of agriculture and water management. One of the most widely used is the adaptation for irrigated crops by [*Tittebrand et al.*, 2005], the Mapping EvapoTranspiration at high Resolution with Internalized Calibration (METRIC) method.

Advantages

- Usually easy to implement as they require few inputs and little local calibration. Data of R_n and T_s is easily obtained from optical and thermal sensors. Additionally, $NDVI$ is available from optical sensors during daytime and clear-sky conditions. G cannot be remotely observed but it is usually estimated as a function of R_n and vegetation properties (see e.g. [*Kustas and Daughtry*, 1990]; [*Bastiaanssen et al.*, 1998]).
- Due to the high resolution of the images traditionally used (e.g. some 120m for LANDSAT), these algorithms have proven very useful for irrigation management.
- Reported good performance of variability methods over semi-arid regions ([*Tang et al.*, 2010]).

Limitations

- Within-image variability is required: i.e. a need for wet and dry pixels within the image. A large number of pixels over a flat area are necessary; they should also show a wide range of soil moisture and fractional vegetation covers.
- In energy-limited regions, the role of temperature as a driver of the vapour pressure deficit often results in a positive correlation between *ET* and T_a (and so T_s) (see e.g. [*Seneviratne et al.*, 2006]) – this contradicts the main assumption of the Triangle Method and reduces its applicability in high latitudes and well-watered regions.
- Image variability methods usually require a rather constant R_n; variations of T_s for a given *NDVI* (in the case of the Triangle Method) or albedo (in the case of S-SEBI) are assumed to occur due to different soil moisture availabilities and not differences in atmospheric forcing. A priori this assumption precludes the direct application of these algorithms over continental domains.
- Due to the need of thermal and optical instantaneous estimates, they only work under clear-sky conditions. This is one of the main reasons why these methods have not been applied at sufficient temporal resolution and over long periods to produce continuous datasets of *ET*.
- These methods usually operate with time averages of instantaneous observations of temperature, which may lead to biased estimates.
- In the case of SEBAL, estimating *H* accurately is key to the success of the approach. However, this estimation relies on the use of the spatial variability of T_s as a proxy for ΔT_a and in the assumptions over the atmospheric stability necessary to estimate r_a. Neither r_a nor the surface level T_a can be directly measured by satellite sensors, and they both vary greatly in space over heterogeneous terrains (see e.g. [*Colaizzi et al.*, 2004]).
- Also in the case of SEBAL, the calculation of *ET* as a residual from eq. (2) and (3) implies that is not constrained by the requirement of energy conservation.

2.3 – One-Source Energy Models

One-source models – as opposed to two-source models (see Sect. 2.4) – treat the soil and the vegetation jointly. They started being developed in the 1980's; see e.g. [*Kalma et al.*, 2008] for a current review. Like SEBAL, these models solve the energy balance (eq. 2) and calculate *ET* as the residual of this equation. However, unlike SEBAL, the methods in this

Box 1. SEBS

In SEBS, like in most of the satellite-based energy balance models, R_n is derived by solving the surface radiation budget based on observations of radiances and T_s; G is derived based on the estimates of R_n and vegetation information. The accuracy of ET estimates becomes set by the skill to derive H. The derivation of H in SEBS is done based on the [*Monin and Obukhov*, 1954]) theory:

$$\theta_0 - \theta_a = \frac{H}{\kappa u_* \rho c_p} \left[\ln\left(\frac{z-d_0}{z_{0h}}\right) - \Psi_h\left(\frac{z-d_0}{L}\right) + \Psi_h\left(\frac{z_{0h}}{L}\right) \right] \tag{4}$$

$$u = \frac{u_*}{\kappa} \left[\ln\left(\frac{z-d_0}{z_{0m}}\right) - \Psi_m\left(\frac{z-d_0}{L}\right) + \Psi_m\left(\frac{z_{0h}}{L}\right) \right] \tag{5}$$

$$L = -\frac{\rho c_p u_*^3 \theta_v}{\kappa g H} \tag{6}$$

where u is the wind speed, u_* is the friction velocity, κ is the von Karman's constant (0.41), z is the height above the surface, d_0 is the zero plane displacement height, z_{0m} and z_{0h} are the roughness heights for momentum and heat transfer, ψ_m and ψ_h are the stability correction functions for momentum and sensible heat transfer respectively. L refers to the Obukhov length, θ_0 is potential land surface temperature and θ_a is the potential air temperature at height z, g is the gravity acceleration and θ_v is the potential virtual air temperature at level z. When the suitable remote sensing, meteorological or reanalysis data are available, the only unknowns are H, u_* and L. This allows the calculation of H and the further estimation of ET based on eq. (2).

Additionally, in order to constrain the H estimates, two limiting cases are considered that set an upper and lower boundary for the evaporative fraction. Under very dry conditions, ET becomes zero and the H is at its maximum, set by $R_n - G$. Under wet conditions, ET occurs at potential rates and therefore H is minimum. In this wet case, H is calculated via reverse application of the Penman-Monteith equation (see Sect. 3.1) assuming that the surface resistance (r_s) is zero. Figure 2 in Sect. 4 outlines a typical flowchart of the SEBS model.

SEBS has been validated against tower measurements and has proved to estimate realistic evaporation rates at a variety of scales ranging from local to regional (see e.g. [*Jia et al.*, 2003]; [*Sheffield*, 2008]; [*McCabe and Wood*, 2006]). Regarding the applicability of SEBS at the continental scale, although the results of recent work within the frame of ESA's WACMOS project were inconclusive (see [*Su et al.*, 2010]), global fields were recently presented by [*Vinukollu et al.*, 2011]. Estimates were validated against measurements of ET from 12 FLUXNET towers in North America (reported for the monthly estimates a *RMSD* of ~1 mm/day, and a 0.51 correlation coefficient). A large-scale operational version of SEBS is currently being tested by Princeton University (Eric Wood personal communication).

category do not have the dependency of within-image variability. This quality potentially increases their applicability for climatological studies.

Presently, the most widely used of these models is the Surface Energy Balance System (SEBS) detailed in [*Su*, 2002] and further developed and applied by [*Su et al.*, 2005] and [*Vinukollu et al.*, 2011] – see Box 1.

Advantages

- The main advantage of methods like SEBS is the detailed characterization of the energy partitioning at the surface level, based on atmospheric and land-surface properties.

Limitations

- The indirect computation of ET as the residual term of eq. (2) potentially implies the propagation of the errors in the calculation of the other terms in the equation.
- The accuracy of ET estimates is again determined by the accuracy of the estimates of H. The parameterization of r_a and ΔT_a – both of them unobservable with satellite sensors – becomes again key for the approach. SEBS for instance makes use of an excess resistance to heat exchange to account for the fact that the T_s observed by satellite sensors is not the required aerodynamic temperature at surface level.
- Usually, they are only available for clear-sky conditions. This limitation is accounted for in [*Vinukollu et al.*, 2011] by running SEBS with reanalyses forcing. Note that virtually all the existing ET methodologies use some form of visible or thermal infrared input datasets (e.g. T_a, R_n).

2.4 – Two-Source Energy Models

One-source models like SEBS treat the whole of the evaporation flux as a bulk – i.e. they do separate different sources of the flux. To avoid this constraint, [*Norman et al.*, 1995] proposed the use of a two-source model that could treat soil and vegetation separately, and therefore provide independent estimates of transpiration and soil evaporation. Two-source models have been further developed by e.g. [*Jupp et al.*, 1998] or [*Kustas and Norman*, 1999].

A good example of this family of models is the Two-Source Time Integrated Model (TSTIM) by [*Anderson et al.*, 1997], later renamed as ALEXI (Atmosphere-Land EXchange Inverse). ALEXI is a two-source land model coupled to a one-dimensional atmospheric boundary layer (ABL) model. Observations of T_s from geostationary satellites are taken at two different times during the morning hours. As in [*Norman et al.*, 1995], estimates of the vegetation cover fraction are used to separate the T_s between soil and vegetation and treat both independently. T_s is used to model T_a and estimate the growth of the ABL and *H*. *G* is again considered as a function of R_n and vegetation. The *ET* from the soil fraction is then derived as the residual from energy balance (just like in SEBAL and SEBS), while the vegetative fraction is first assumed to evaporate at potential rate (estimated using the Priestley and Taylor (PT) equation), and corrected afterwards to keep the energy balance closure. ALEXI has already been applied at the large scale in order to map *ET* over the entire USA ([*Anderson et al.*, 2007]) and its applicability to other regions is feasible provided the availability of the required geostationary data [*Anderson et al.*, 2011].

Advantages

- The parameterization of the growth of the ABL potentially improves the skill of these models to derive water and energy fluxes at sub-daily time scales.
- In models that integrate an ABL formulation, like ALEXI, T_a is derived (and not observed): biases in the observations of T_s are not propagated to the estimates of ΔT_a required to derive *H*.
- No local calibration is required and, if coupled to the ABL growth, no observations of T_a are required either.
- They are prone to work better than one-source models where there is a heterogeneous land cover and there are large differences between soil and canopy temperatures.

Limitations

- They require geostationary T_s observations under clear-sky conditions and early morning sounding to determine the lapse rate.
- The complexity and large input requirements complicate the applicability of these algorithms over larger domains to produce continuous long-term climatological records.

3 – Algorithms reported for continental and global scales

3.1 – Penman Monteith approaches

The Penman Monteith (PM) equation by [*Monteith*, 1965] has long been recognized as one of the most accurate formulas to derive *ET* (see e.g. [*Allen et al.*, 1998]). The PM equation extends the [*Penman*, 1948] open water evaporation formulation to vegetated surfaces by considering: (a) the stomatal water vapour is saturated at the leaf temperature, (b) the leaf surface is at the vapour pressure of the surrounding air, (c) there is a resistance that controls the transfer of vapour from the leaf to the surrounding air, and (d) the leaf resistance is integrated up to the canopy resistance. The resulting PM equation can be expressed as:

$$ET = \frac{\Delta(R_\mathrm{n} - G) + \rho c_\mathrm{p} VPD / r_\mathrm{a}}{\lambda\left[\Delta + \gamma\left(\frac{r_\mathrm{s}}{r_\mathrm{a}}\right)\right]} \tag{7}$$

where *VPD* is the vapour pressure deficit, γ is the psychrometric constant and r_s is the surface resistance.

The PM equation does not partition *ET* between the contributing sources of soil evaporation, interception loss, sublimation and transpiration. However, more detailed structural forms of eq. (7) have been developed with consideration of *ET* in different layers and/or sources, often targeted for field-scale estimations of *ET* (e.g. [*Shuttleworth and Wallace*, 1985]; [*Farahani and Ahuja*, 1996]; [*Brenner and Incoll*, 1997]; [*Lhomme et al.*, 2012]).

The characterization of the resistances from soil and canopy (here referred jointly as r_s) makes the application of any form of the PM equation problematic, especially if these resistances are to be inferred from satellite data only. Recently, [*Cleugh et al.*, 2007] made a consistent remotely sensed-based dataset of *ET* centered on a PM approach by deriving r_s empirically. They related r_s to satellite-derived Leaf Area Index (*LAI*) and fraction of canopy cover using data from the MODerate Resolution Imaging Spectroradiometer (MODIS). Their results were presented at a 1km resolution over Australia. Later modifications of this methodology have investigated other ways to calibrate the PM model for its application to MODIS data ([*Mu et al.*, 2007]; [*Leuning et al.*, 2008]; [*Zhang et al.*, 2010a]). Particularly, [*Mu et al.*, 2007] extended the approach by adding other environmental controls over r_s, like water vapour deficit, and computing estimates of soil evaporation separately. Subsequently, [*Mu et al.*, 2011] also included a parameterization for rainfall interception loss (see Box 2).

[*Leuning et al.*, 2008] presented a series of modifications of the algorithm by [*Cleugh et al.*, 2007] that were then applied by [*Zhang et al.*, 2008] to several catchments over Australia. The application was later extended to the global scale making use of R_n from SRB, *NDVI* data from AVHRR and re-analyses data ([*Zhang et al.*, 2010b, 2012]). Global fields were produced spanning from 1983 to 2006 at 8 km spatial resolution.

Finally, [*Sheffield et al.*, 2010] applied the algorithm by [*Mu et al.*, 2007] to the datasets from ISCCP ([*Zhang et al.*, 2004]), making use of wind speed from re-analyses ([*Sheffield et al.*, 2006]) to derive r_a. Estimates of *ET* were evaluated over Mexico, and a 1986-2006 daily global dataset at 2.5° resolution was developed in a later stage.

Box 2. PM-Mu

[*Mu et al.*, 2011] recently extended the [*Mu et al.*, 2007] model by representing *ET* as the sum of transpiration (ET_t), evaporation from the soil (ET_s) and interception loss (I):

$$ET = ET_t + ET_s + I \tag{8}$$

where I is modeled as:

$$I = f_{wet}\, f_c \; \frac{\Delta(R_n - G) + \rho c_p VPD / r_a^{wc}}{\lambda\left(\Delta + \gamma \dfrac{r_s^{wc}}{r_a^{wc}}\right)} \tag{9}$$

f_c is the canopy fraction, f_{wet} is the wet cover fraction (based on the derivation by [*Fisher et al.*, 2008] – see Box 3) and r_a^{wc} and r_s^{wc} are aerodynamic and surface resistances against evaporation of the intercepted water (calculated as functions of T_a and *LAI*).

Canopy transpiration ET_t is estimated as:

$$ET_t = (1 - f_{wet})\, f_c \; \frac{\Delta(R_n - G) + \rho c_p VPD / r_a^{t}}{\lambda\left[\Delta + \gamma\left(\dfrac{r_s^{t}}{r_a^{t}}\right)\right]} \tag{10}$$

where r_a^t and r_s^t are the aerodynamic and surface resistances against transpiration. r_a^t is determined in a similar way to r_a^{wc}, and r_s^t is a function of stomatal conductance, biome-constant values of cuticular conductance and canopy boundary layer conductance. The values of stomatal conductance are a function of T_a, *VPD* and *LAI*.

Evaporation from the soil surface (ET_s) is the sum of evaporation from wet soil and evaporation from saturated soil, which are both calculated separately based on the PM equation with specific values of r_a, r_s for bare soils and a soil moisture constrain (f_{sm}) based on relative humidity (also taken from [*Fisher et al.*, 2008] – see Box 3).

The PM-Mu algorithm requires vegetation characteristics (e.g. AVHRR or MODIS), wind speed, humidity, air pressure, R_n, T_a and T_s. Since not all inputs are available from remote sensing systems, reanalysis data have been used in some instances instead (see [*Mu et al.*, 2007], [*Mu et al.*, 2011]). Estimates have been successfully validated against measurements of *ET* from 46 FLUXNET towers in North America (reported for the daily estimates a *RMSD* of 0.91 mm/day, and a 0.53 correlation coefficient). More details about the model requirements are given in Table 1 and a flowchart of the methodology is presented in Figure 3.

Advantages

- More robust physical basis (as opposed to the PT method). It considers not only the radiation forcing on *ET* but also atmospheric feedbacks on *ET* via humidity and air temperature.

– Direct estimation of *ET* (as opposed to many energy balance models).

Limitations

– The main limitation is the requirement of a large number of variables that are either difficult to observe (e.g. near surface humidity) or not observable (e.g. wind speed over land) with satellites. This demands the use of meteorological or atmospheric reanalysis data as inputs to the algorithms.

– The theoretical advantage of PM over PT of having a more physically-based parameterization of the surface conductance becomes hampered by the inability to measure this conductance from satellites. The characterization of r_s needs to be based on proxies and therefore is not substantially different from other empirical stress functions commonly applied to ET_p estimates via PT equation (see Sect. 3.2).

– Current global PM algorithms do not consider soil moisture but atmospheric humidity as a surrogate for surface water stress.

3.2 – Priestley and Taylor approaches

ET can be obtained from infrared and visible data via the (PT) [*Priestley and Taylor*, 1972] equation:

$$ET_p = \alpha \frac{1}{\lambda} \frac{\Delta (R_n - G)}{\Delta + \gamma} \tag{11}$$

where α is known as the PT coefficient and is usually considered as a constant value that aims to summarize the atmospheric term in the PM equation (Sect. 3.1). T_a observations play a role in the calculation of the slope of the saturation vapour pressure curve (Δ), and can also be used to determine the latent heat of vaporization (λ) and the psychrometric constant (γ). To derive *ET*, the PT estimates of ET_p need to be modified to consider the actual evaporative stress (i.e. the deviation from potential conditions of sufficient soil water availability and optimal physiological activity inherent in the definition of ET_p).

The first applications of PT equation to remote sensing data were undertaken at regional scales. [*Barton*, 1979] derived an empirical stress factor using soil moisture data from microwave sensors over bare soils (this factor was used to modify Δ). As described in Sect. 2.2, the use of the Triangle Method (i.e. *NDVI* vs. T_s) has also been proposed to derive the evaporative stress in combination with ET_p estimates from eq. (11) (see e.g. [*Jiang and Islam*, 2001]). [*Venturini et al.*, 2008] derived a factor to correct Δ in an analogous way to [*Barton*, 1979], but instead of using soil moisture content, they accounted for air and surface vapour pressure based on different remotely-sensed temperatures – [*Venturini et al.*, 2008; *Venturini* *et al.*, 2011] presented gridded fields of *ET* for a region of the Great Plains (US) using data from MODIS Terra. This methodology shows realistic spatial variability at high resolutions; however, the applicability becomes again subjected to within-image variability in cloud-free images; whether it can be used to produce a continuous long-term record of *ET* is still under question.

The first application of the PT equation at the global scale to create a climatological record of *ET* from remote sensing observations is due to [*Fisher et al.*, 2008]. Several multipliers (ranging from 0 to 1) based on vapour pressure deficit, relative humidity, *NDVI* and *SAVI* (soil adjusted vegetation index) were proposed to adapt the PT equation to account for evaporative stress (see Box 3). Global monthly fields were produced from 1986 to 1995 at a 0.5° resolution using data from the ISLSCP-II. [*Vinukollu et al.*, 2011] have recently inter-compared the product by [*Fisher et al.*, 2008], SEBS and the PM model by [*Mu et al.*, 2007] at a daily time scale and 5 km spatial resolution.

Finally, [*Miralles et al.*, 2011b] proposed an algorithm – named GLEAM (Global Land-surface Evaporation: the Amsterdam Methodology) – that separately calculates transpiration, soil evaporation, open water evaporation and sublimation based on a modified PT equation. Rainfall interception loss is estimated based on the Gash analytical model ([*Gash*, 1979]; [*Valente et al.*, 1997]). A multiplicative evaporative stress factor is derived by combining microwave data of vegetation optical depth (a proxy for vegetation water content) and soil moisture (see Box 4). Estimates have been validated and evaluated at the global scale ([*Miralles et al.*, 2010; *Miralles et al.*, 2011a; *Miralles et al.*, 2011b]), and the methodology is currently being adapted to the regional scales by improving the realism of the soil module. Daily global fields at a 0.25° resolution are available from 1984 to 2007 and are recently being used for the study of land-atmosphere interactions (e.g. [*Miralles et al.*, 2012]).

Advantages

- The PT equation is well-suited for remote sensing data: it retains the energy-driven part of the PM equation that is the more easily derived using the current range of observable variables. The estimation becomes feasible when only observations of R_n and T_a are available.
- They provide direct estimation as opposed to energy balance models.

Limitations

- Neither the water vapour deficit nor the surface and aerodynamic resistances (r_a, r_s) are explicitly accounted for.

- In regions of strong advection (some coastal and semiarid climates), the performance of the models in prone to larger errors; better estimates in those regions may require a dynamic estimation of α.
- Strong dependency on R_n. The PT equation implies no evaporation when the available energy is lower or equal to zero.

Box 3. PT-JPL

The algorithm by [*Fisher et al.*, 2008] is based upon the *PT* equation (eq. 2). To constrain ET_p, it uses a number of eco-physiological constraint functions with values between 0-1 (unitless multipliers referred to as *f*-functions). These are based on atmospheric humidity (*VPD* and relative humidity, *RH*) and vegetation indices (*NDVI* and *SAVI*).

The driving equations in the model are:

$$ET = ET_t + ET_s + I \tag{11}$$

$$ET_t = (1 - f_{wet})\, f_g\, f_T\, f_M\, \alpha \frac{\Delta}{\lambda(\Delta+\gamma)} R_n^c \tag{12}$$

$$ET_s = \left[f_{wet} + f_{sm}(1 - f_{wet})\right]\alpha \frac{\Delta}{\lambda(\Delta+\gamma)} (R_n^s - G) \tag{13}$$

$$I = f_{wet}\, \alpha \frac{\Delta}{\lambda(\Delta+\gamma)} R_n^c \tag{14}$$

where f_{wet} is the relative surface wetness ($f_{wet} = RH^4$), f_g is green canopy fraction (f_g = fAPAR/ fIPAR, where fAPAR is the fraction of absorbed and fIPAR is the fraction of intercepted photosynthetically active radiation), f_M is a plant moisture constraint (f_M = fAPAR/ fAPAR$_{max}$), f_{sm} is a soil moisture constraint ($f_{sm} = RH^{VPD}$) and f_T is a plant temperature constraint defined as:

$$f_T = e^{-\left(\frac{T_a - T_{opt}}{T_{opt}}\right)^2} \tag{15}$$

T_{opt} is the optimum plant growth temperature, estimated as the air temperature at the time of peak canopy activity when the highest f_{APAR} and minimum *VPD* occur. Ultimately, the requirements to drive the algorithm are R_n, T_a, atmospheric humidity and vegetation indices. These may be obtained from in-situ measurements, reanalyses or remote sensing products.

Specific details of the model can be found in [*Fisher et al.*, 2008]. It has been tested against measured *ET* from 16 FLUXNET sites worldwide (reported monthly average *RMSD* of ~0.4 mm/day, and a ~0.94 correlation coefficient). Figure 4 provides a schematic of the algorithm structure and the required inputs.

Box 4. GLEAM

It calculates *ET* via PT, a soil moisture-stress computation and a Gash analytical model of rainfall interception loss ([*Gash*, 1979]). In the absence of snow, evaporation from land is calculated as:

$$ET = ET_{\mathrm{tc}} + ET_{\mathrm{sc}} + ET_{\mathrm{s}} + \beta I \qquad (16)$$

in which ET_{tc} is transpiration from tall canopy, ET_{sc} is transpiration from short vegetation, ET_{s} is soil evaporation and *I* is tall canopy interception loss. β is a constant used to account for the times in which vegetation is wet and so transpiring at lower rates (β = 0.93 – [*Gash and Stewart*, 1977]).

The first three terms in eq. (9) are derived using the PT equation, so *ET* becomes:

$$ET = \frac{\Delta\left[f_{\mathrm{tc}}\, S_{\mathrm{tc}}\, \alpha_{\mathrm{tc}}(R_{\mathrm{n}}^{\mathrm{tc}} - G_{\mathrm{tc}}) + f_{\mathrm{sc}}\, S_{\mathrm{sc}}\, \alpha_{\mathrm{sc}}(R_{\mathrm{n}}^{\mathrm{sc}} - G_{\mathrm{sc}}) + f_{\mathrm{s}}\, S_{\mathrm{s}}\, \alpha_{\mathrm{s}}(R_{\mathrm{n}}^{\mathrm{s}} - G_{\mathrm{s}})\right]}{\lambda(\Delta + \gamma)} + \beta I \qquad (17)$$

where the subscripts *tc*, *sc* and *s* correspond to tall vegetation, short vegetation and bare soil respectively. The fraction of each cover type per pixel is represented by *f* and *S* represents the evaporative stress due to soil moisture deficit and vegetation phenology. Different cover types have different values of α and parameterizations of *G* and *S* (e.g. vegetation optical depth is not use to compute *S* in bare soils, and the root-zone depth and layers depend also on the land cover). Additionally, R_{n} is distributed within the cover fractions using ratios of albedo from the literature.

Soil moisture deficit is parameterized using a multilayer running water balance to describe the infiltration of *P* through the vertical soil profile. Microwave surface soil moisture observations are assimilated into the top soil. The goal is to convert observations of *P* and surface soil moisture into estimates of root-zone soil water content. To consider the effects of phenological changes on *ET*, the conversion of root-zone soil moisture into *S* is done in combination with observations of vegetation water content (i.e. microwave vegetation optical depth – [*Liu et al.*, 2011]).

I is independently derived using a Gash analytical model, in which a running water balance for canopies and trunks driven by precipitation (*P*) observations. The derivation of the parameters, global implementation, and validation of this *I* model is described in [*Miralles et al.*, 2010].

For regions covered by ice and snow, sublimation is calculated based on a PT equation run with parameters calibrated for ice and super-cooled waters ([*Murphy and Koop*, 2005]). Open water evaporation is assumed to be PT potential evaporation and calculated using specific values of albedo and ground heat flux for open water.

The main features are the consideration of soil moisture, the separate parameterization of interception loss and the extensive use of microwave observations. The main limitation is the non-consideration of near-surface atmospheric humidity (justified by the fact that it cannot be observed with satellites). The *ET* product has been validated 43 FLUXNET stations world wide (reported yearly average *RMSD* of ~0.3 mm/day, and a ~0.8 correlation coefficient), the *I* has been compared to estimates from 42 field studies in different forest ecosystems, and the error structure of the *ET* estimates has been analysed using triple collocation ([*Miralles et al.*, 2010], [*Miralles et al.*, 2011a], [*Miralles et al.*, 2011b]). Figure 5 in Sect. 4 presents the flowchart of the model.

3.3 – Empirical approaches

Remote sensing data can be used to up-scale micrometeorological measurements from the local to the regional/global scale. [*Wang and Liang*, 2008] proposed an empirical method based on a linear regression between R_n, T_a, T_s and *NDVI* to upscale the fluxes measured at eight meteorological stations in the Great Plains (US). The model was then extended to global scale and monthly temporal resolution by using data from the International Satellite Land-Surface Climatology Project, Initiative II (ISLSCP-II): R_n from the Surface Radiation Budget (SRB, GEWEX) ([*Stackhouse et al.*, 2004]), daily averaged and diurnal range of the T_a from the Climate Research Unit (CRU) ([*New et al.*, 2000]) and a vegetation index from the AVHRR reflectances ([*Gutman*, 1999]). [*Wang et al.*, 2010a; *Wang et al.*, 2010b] further developed the model by including the impact of wind speed and water vapor pressure deficit.

[*Jung et al.*, 2009] presented a machine-learning algorithm – the model tree ensembles (MTE) – to estimate *ET* using eddy covariance measurements from FLUXNET ([*Baldocchi et al.*, 2001]). *In situ* measurements were corrected at monthly scale to force the closure of the energy balance. The remote sensing data used for the up-scaling covered different datasets of photosynthetically active radiation (fAPAR), T_a from CRU, *P* from the Global Precipitation Climatology Center (GPCC) ([*Rudolf and Schneider*, 2005]) and an estimate of the top of the atmosphere shortwave radiation. The model was run at a spatial resolution of 0.5° and monthly time scale from 1982 to 2008. Based on this algorithm, [*Jung et al.*, 2010] presented the first comprehensive observational-based study of the trends in global *ET* over the last three decades.

To conclude, [*Jiménez et al.*, 2009] proposed a similar empirical methodology, but instead of using *in situ* measurements, global fluxes from several land surface models were applied to calibrate different empirical relationships using satellite data. This approach has proved to effectively merge the information from the remote sensing observations with the land surface models, similar to other assimilation approaches (e.g. [*Aires and Prigent*, 2006; *Aires et al.*, 2005]).

Advantages

- Relatively simple formulations.
- The explicit use of *in situ* measurements can potentially increase the accuracy.
- Large degree of independency relative to more physically-based methodologies.

Limitations

- The use of *in situ* measurements (e.g. FLUXNET) in the derivation of *ET* implies that these same measurements cannot be applied for the validation of the algorithms.

- Lack of physics in the method's rationale.
- Some have been derived specifically for climatological studies and present a monthly temporal resolution which seems insufficient for some agricultural and water management applications.

4 – Overall Assessment and Pre-Selection of Algorithms

WACMOS-ET aims to advance the improvement and characterization of *ET* estimates from satellite observations at continental and regional scales; a cross-comparison, error assessment, and validation exercise of a selection of state-of-art algorithms will be undergone in the project. Sections 2 and 3 have analyzed the advantages and disadvantages of the currently existing algorithms. Here we present the subset of this range of algorithms that will constitute the basis of upcoming activities within WACMOS-ET.

We have considered six criteria in the pre-selection. The algorithms should:

1) have been applied in the past over either regional or continental scale, and preferably over both scales
2) have proven skill to produce long-term continuous data records of *ET*
3) have low requirements in ancillary data that cannot be observed or derived from satellites
4) need low levels of local calibration, which eases the transferability of the methods from region to region and from scale to scale
5) be designed to run at least at daily temporal resolution
6) be based on satellite and not *in situ* observations as the core of their approach

Additionally, the algorithm developers must have communicated to us their willingness to either share their algorithms or contribute more actively to the activities of the project.

In the case of local to regional scale empirical approaches, like the Simplified Method (Sect. 2.1) and the within-image variability techniques (Sect. 2.2), the main limitations are the unproven skill of the algorithms to produce a continuous record of *ET*, and the unclear applicability of these methods to larger scales. These disadvantages mainly come from the reliance of these methods on instantaneous cloud-free images and the requirements of substantial levels of local calibration. On the other hand, the empirical approaches by [*Wang and Liang*, 2008], [*Jiménez et al.*, 2009] or [*Jung et al.*, 2009] (see Sect. 3.3), have been designed (or successfully adapted) to work at larger spatial scales. Even though these are powerful approaches with a large degree of independency and interesting potential for hydrological and climatological analysis, they are limited in their applicability to regional scales: they either rely on meteorological measurements as the basis of the approach or their adaptability to daily temporal resolution is still under question. Nevertheless, as part of the activities within WACMOS-ET, the applicability of the MTE algorithm ([Jung et al., 2009]) at the required daily time-scales will be examined. If the model is successfully adapted to daily time scales, the inclusion of this algorithm in our activities will provide *ET* estimates with a very different error structure than the ones derived via process-based algorithms.

More complex two-source energy balance algorithms (see Sect. 2.4) provide a detailed parameterization of land-atmosphere interactions and are built on comprehensive physics. Their adaptability from region to region is however cumbersome, partly due to their extensive requirements in terms of input data. ALEXI – which currently represents the most widely used of these approaches – has already been adapted to map *ET* over large domains (e.g. Anderson et al., 2007). The applicability of ALEXI to other large regions is currently being examined (Martha Anderson and Christopher Hain personal communication); the final inclusion of ALEXI in the activities of WACMOS-ET will depend of the success of this exercise. The ALEXI science team has however communicated their interest in participating in the activities of WACMOS-ET as long as the algorithm is ready by the beginning of the phase 3 of the project (November 2013).

SEBS, the one-source energy balance algorithm by [*Su*, 2002], later adapted by [*Su et al.*, 2005] and [*Vinukollu et al.*, 2011], is arguably the most widely used energy balance approach in the present. It has been successfully applied to produce long-term *ET* records at scales from regional to global (e.g. [*McCabe and Wood*, 2006]; [*Vinukollu et al.*, 2011]). The algorithm meets all the requirements specified above for its inclusion in WACMOS-ET activities. Contact with the developer's team has been made and we currently have an operational code of SEBS and the authorization to use it within the activities of the project.

The PT and PM approaches presented in Sect. 3.1 and 3.2, represent a rather direct process-based estimation of *ET*; unlike the estimation of *ET* through energy balance models, these algorithms do not require the explicit derivation of H and therefore avoid problems associated with the definition of a vertical gradient of T_a. The main advantage of these approaches is that most of their core equations were derived in past regional-scale experiments, often targeting at agricultural and water management applications (e.g. [*Priestley and Taylor*, 1972]), but at the same time the recent application over larger scales (e.g. global) means that there is also experience facing the challenges that these algorithms pose over these scales (e.g. the global derivation of surface resistance for PM, or global stress factors for PT). This flexibility also implies that local calibration is less of a necessity and more of an alternative to improve their regional performance. Finally, the fundamental and simple physics behind these approaches guaranties a certain level of performance at both regional and global scales provided the existence of forcing data with the appropriate resolution and accuracy. We have contacted the model developers of the PM-Mu and PT-JPL algorithms (see Box 2 and 3) and they are willing to collaborate in the WACMOS-ET activities.

Finally, the WACMOS-ET team hosts the latest version of GLEAM (see Box 4), which we believe will add a rather independent approach to the estimation of *ET* and strengthen WACMOS-ET activities. The main difference of GLEAM from PM-Mu and PT-JPL, is that the evaporative stress is based on (microwave) soil moisture instead of air humidity factors. However, the requirement of soil related properties complicates its applicability to more local scales and the team is currently working towards the adaptability of the method at point-scale.

Therefore, our 4 pre-selected algorithms are: SEBS ([*Su*, 2002], [*Vinukollu et al.*, 2011]), PM-Mu ([*Mu et al.*, 2011]), PT-JPL ([*Fisher et al.*, 2008]) and GLEAM ([*Miralles et al.*, 2011b]). In addition, the inclusion of MTE ([Jung et al., 2009]) will depend on the success of its adaptation to daily scales, and the inclusion of ALEXI ([*Anderson et al.*, 1997]) will depend on the progress of the ALEXI research team in coming months towards the applicability of the method over the 4 study sites selected for the WACMOS-ET project. All these methodologies are suitable for both regional and continental scales, and appropriate for both agricultural and climatological applications. Their spatial resolution ranges from near-point scale, when run with meteorological data, to scales of fractions of a degree when run with remote sensing data – i.e. the spatial resolution ultimately depends on the forcing datasets used to drive the algorithms.

Figures 2-5 show the schematics of the 4 pre-selected algorithms, and how the different inputs are combined within each methodology – note that the degree of complexity of the algorithms is not necessarily proportional to the number of variables and interactions in these figures. Table 2 summarizes some of the main differences among these 4 pre-selected schemes that have already been discussed in Box 1-4. Table 3 list some other published global products discussed here that may be run as part of the project depending on successful product development (i.e., ALEXI and MTE), or that will not be explicitly run as part of the project. Finally, Table 4 provides a summary of the input variables required to run each of these algorithms together with the specific datasets that have been used as inputs in past applications (e.g. [*Vinukollu et al.*, 2011]; [*Mu et al.*, 2011]; [*Fisher et al.*, 2008]; [*Miralles et al.*, 2011b]). Note that these algorithms are rather flexible as to the specific products used as forcing data (so relatively simple adaptation to the specific common forcings of the project Reference Input Dataset is expected) and that better quality datasets of the required variables should also imply higher quality *ET* estimates.

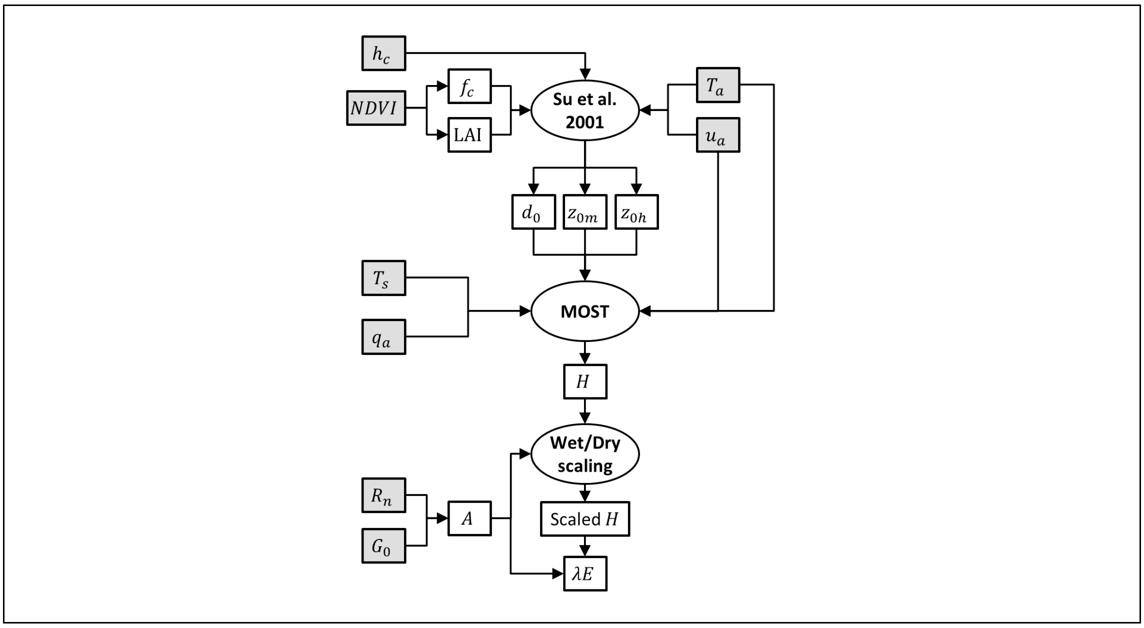

Figure 2 – Flowchart of the SEBS algorithm (after [*Su*, 2002] and [*Vinukollu et al.*, 2011]).

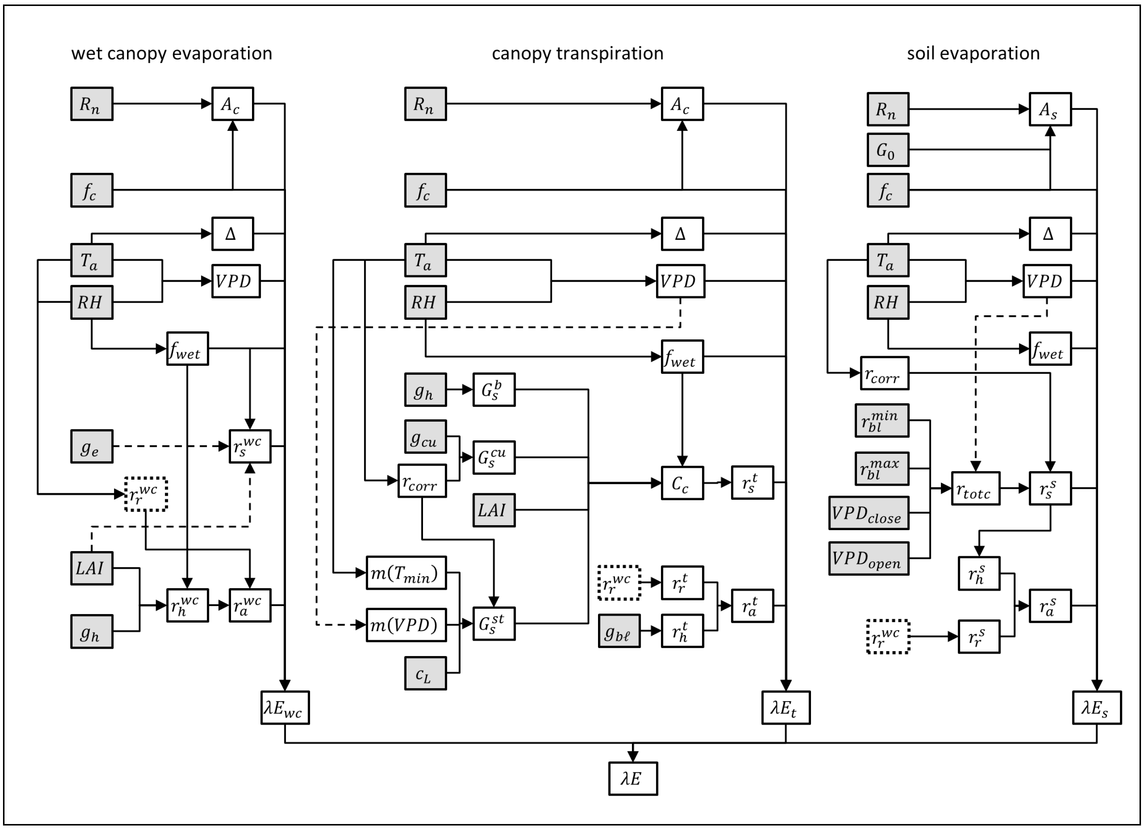

Figure 3 – Flowchart of the PM-Mu algorithm (after [*Mu et al.*, 2011]).

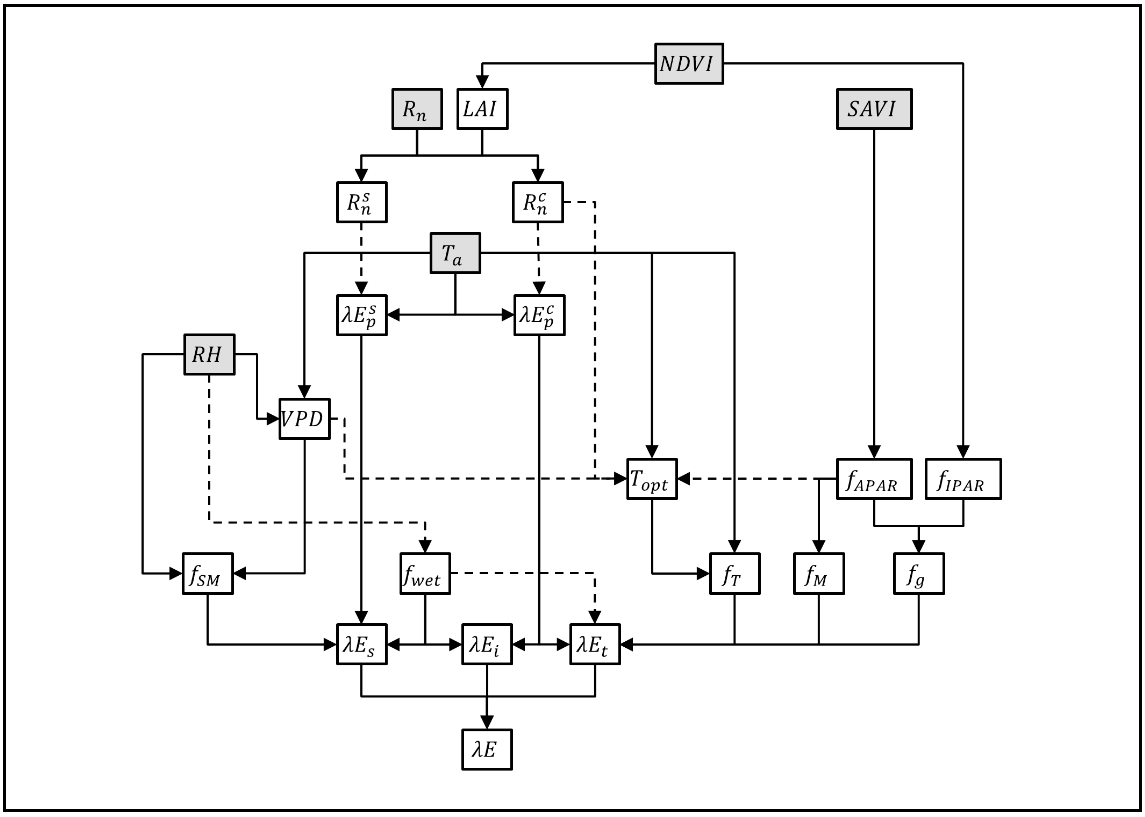

Figure 4 – Flowchart of the PT-JPL algorithm (after [*Fisher et al.*, 2008]).

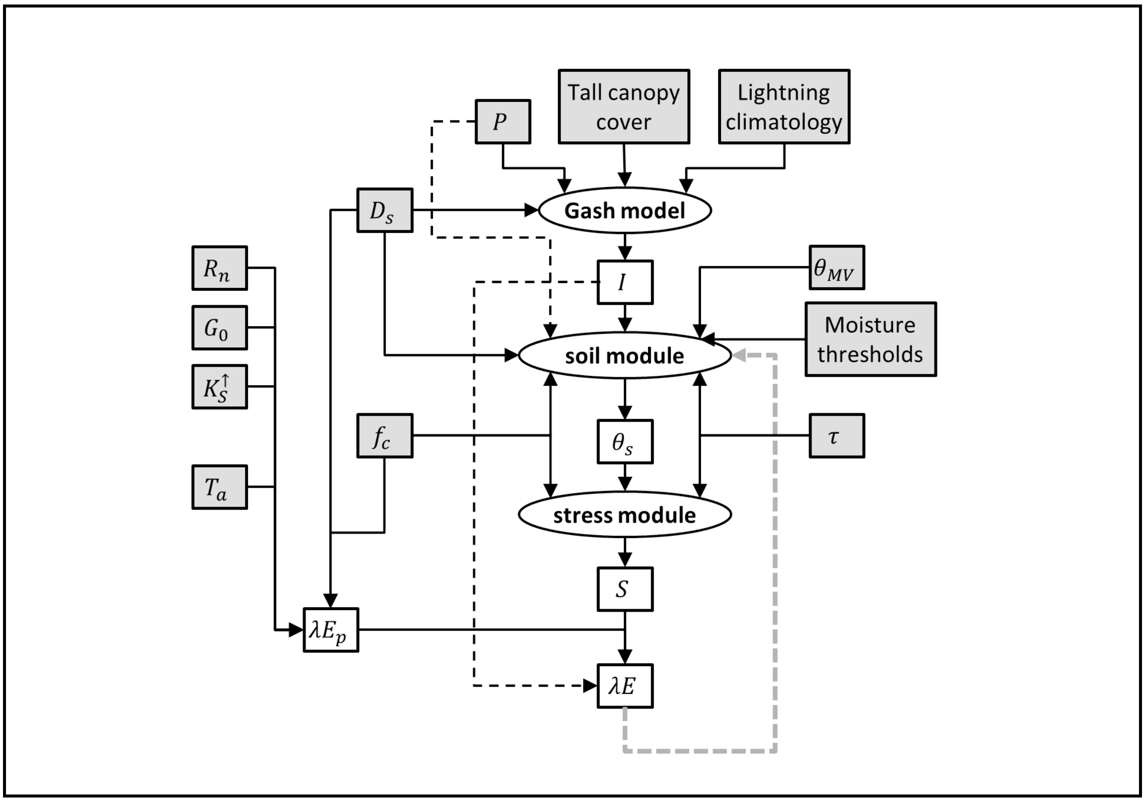

Figure 5 – Flowchart of the GLEAM algorithm (after [*Miralles et al.*, 2011b]).

PRODUCT	METHOD	INTERCEPTION	SUBLIMATION	GROUND FLUX	DATASET
SEBS [*Su*, 2002] as run by [*Vinukollu et al.*, 2011]	*ET* as residual of the surface energy balance after estimation of *H* from vertical gradient of T_a	Incorporated in [*Vinukollu et al.*, 2011] based on [*Valente et al.*, 1997] and PT equation	Penman equation as in [*Calder*, 1990]	As function of R_n with interpolation based on fractional canopy coverage	Global Daily 0.5° x 0.5° 1984-2007
PM-Mu [*Mu et al.*, 2011]	PM formulation with biome-specific canopy conductance	Modeled by PM using specific wet canopy resistances	Not explicitly modeled	As function of temperature	Global 8-day 1km x 1km 2000-2012
PT-JPL [*Fisher et al.*, 2008]	PT formulation with stress factors based on biophysical metrics	PT equation multiplied by fraction of time with wet surface	Not explicitly modeled	Assumed to be zero	Global Monthly 0.5° x 0.5° 1983-2007
GLEAM [*Miralles et al.*, 2011b]	PT with stress based on soil moisture and vegetation water content; Gash model of interception loss	Analytical model by [*Gash*, 1979] and [*Valente et al.*, 1997] (see [*Miralles et al.*, 2010])	PT equation with snow adapted variables from [*Murphy and Koop*, 2005]	As function of R_n and fractional canopy coverage	Global Daily 0.25° x 0.25° 1984-2007

Table 2 – Comparison of the pre-selected algorithms and major differences in their parameterization. The right column indicates the domain, period and resolution that the models have been run in the corresponding citation (see left column).

PRODUCT	METHOD	INTERCEPTION	SUBLIMATION	GROUND FLUX	RESOLUTION
[Zhang et al., 2010a]).	PM model with biome-specific canopy conductance	NEM	NEM	As function of Rn with biome specific constants	Daily 8km x8km 1983-2006
[Sheffield et al., 2010]	PM model wih biome specific canopy conductance	NEM	NEM	Predicted from lagged change in Ts Tsuang (2005)	Daily 2.5° x 2.5° 1986-2006
[Zhang et al., 2012]	PM model with biophysical canopy conductance and catchment water –balance calibration	NEM	NEM	Not modelled, assumed ~0	Monthly 0.5° x 0.5° 1983-2006
[Anderson et al., 2007] ALEXI	Morning surface temperature rise in a TSEB model coupled with an ABL model and water pools for cloud gap-filling	NEM	NEM	Fixed fraction of Rs (soil net radiation)	From sunrise+5h to hourly or daily 10 km (only over US) 2000-present
[Wang and Liang, 2008]	Semi-empirical model calibrated with ground-based tower measurements	NEM	NEM	NEM	Monthly 1° x 1° 1986-2005
[Jiménez et al., 2009]	Empirical model calibrated developed with land surface model estimates	NEM	NEM	NEM	Monthly 0.25° x 0.25 1993-1995
[Jung et al, 2010] MTE	Empirical model calibrated with ground-based tower measurements	NEM	NEM	NEM	Monthly 0.5° x 0.5 1982-2008

Table 3 – Comparison of some other published global satellite-based *ET* products not listed in Table 2 and of relevance for this work. Notice that ALEXI is not a global product (it is included as it can potentially be run as part of the project). Notice also that [Jung et al., 2010] is not strictly a satellite *ET* product as it is to a large extent based on products derived by global extrapolation of ground measurements (it could also potentially be run as part of the project after successful adaptation to the project inputs and the required daily scale). The table format is as in Table 2.

		NET RADIATION (R_n)
SEBS	NASA/GEWEX SRB 3.0	3-hourly net shortwave (SW) and net longwave (LW) fluxes, downscaled from 1° to 0.5° grid
PM-Mu	MERRA GMAO	Daily down-welling SW fluxes, from 0.5° x 0.6° grid to 1km MODIS pixels; upwelling SW using MODIS albedo, net LW flux from T_a and estimates of surface and air LW emissivity
PT-JPL	NASA/GEWEX SRB	Monthly net SW & LW fluxes, from 1° to 0.5° grid
GLEAM	NASA/GEWEX SRB 3.0	Daily net SW & LW fluxes, from 1° to 0.25° grid
		SURFACE TEMPERATURE (T_s)
SEBS	VIC land-surface model [*Sheffield and Wood*, 2007]	To estimate air temperature gradient between the surface and overlying atmosphere (ΔT_a)
		SURFACE SOIL MOISTURE (θ)
GLEAM	LPRM v04d [*Owe et al.*, 2008]	Assimilated with the *P*-derived water content of the first layer in the soil water module; based on microwave observations from different sensors (i.e. SMRR, SSMI, TRMM, AMSR-E)
		PRECIPITATION (*P*)
GLEAM	CMORPH [*Joyce et al.*, 2004]	Daily precipitation as input to water budget module, separated into rain and snow by snow-depth observations; scaled from 0.07° to 0.25°, GPCP-1DD 4.0 to gapfill outside the domain 60S-60N; snow-depth from NSIDC AMSR-E/Aqua daily L3 v001 ([*Kelly et al.*, 2003])
		AIR TEMPERATURE (T_a)
SEBS	Princeton forcing [*Sheffield et al.*, 2006]	To estimate temperature gradient between the surface and overlying atmosphere (ΔT_a) NCEP-NCAR temperature bias-corrected with CRU TS 2.0
PM-Mu	MERRA GMAO	To estimate LW flux, Δ, *VPD* as function of T_a, and to parameterize soil conductance (resolutions as described for the radiative fluxes)
PT-JPL	CRU TS 3.0	To estimate Δ and f_T ; at 0.5°x0.5° resolution
GLEAM	ISCCP / AIRS	Use of AIRS for the period 2003-2007; ISCCP for gap-filling and before 2003; used to estimate Δ and to blend CMORPH and GPCP-1DD *P*
		WIND SPEED (*u*)
SEBS	Princeton forcing [*Sheffield et al.*, 2006]	To estimate r_a ; downscaled from ~2.0° to 0.5°
		WATER VAPOR PRESSURE
PM-Mu	MERRA-GMAO	To estimate *VPD* and *RH* for the calculation of f_{wet} and f_{sm} (resolutions as described for R_n)
PT-JPL	CRU TS 3.0	To estimate *VPD* and *RH* for the calculation of f_{wet} and f_{sm}; monthly 0.5°x0.5°
		VEGETATION INDEX
SEBS	AVHRR [*Tucker et al.*, 2005]	*NDVI*, *LAI* to derive the fractional vegetation cover and other parameters to be used in the determination of surface roughness height; at 8 km and 15-days resolution
PM-Mu	NASA MODIS	*FPAR* for fractional cover, *LAI* to estimate canopy conductance; gapfilled as in [*Zhao et al.*, 2005]
PT-JPL	NASA MODIS	*NDVI*, *EVI* to estimate fraction of photosynthetic active radiation absorbed by green and total vegetation and derive green canopy fraction and plant moisture constraint
GLEAM	LPRM v04d based on AMSR-E MW	Microwave vegetation optical depth as a proxy for vegetation water content, at 0.25°; Only applied to vegetated fractions of grid pixel to estimate the phenology component of *S*
		LAND COVER / SOIL PROPERTIES
SEBS	MODIS-based land cover (MOD12Q1)	For land mask, no biome-specific parameters
PM-Mu	MODIS Col. 4 [*Friedl et al.*, 2010]	To determine land cover and fractional vegetation type, including 11 vegetation types
PT-JPL	ISLSCP	For land mask, no biome-specific parameters
GLEAM	MOD44B [*Hansen et al.*, 2005] IGBP-DIS [*Global Soil Data Task Group*, 2010]	Vegetation continuous fields from MODIS (MOD44B) to describe every pixel as a combination of tall canopy, short vegetation and bare soil. IGBP-DIS to define available soil water thresholds (wilting point, critical soil moisture and field capacity)

Table 4 – Summary of the input variables required to run each of the pre-selected algorithms and the specific preferential datasets used in past applications of these algorithms – e.g. [Vinukollu et al., 2011], [Mu et al., 2011], [Fisher et al., 2008] or [Miralles et al., 2011b]. Note that these algorithms are rather flexible; better datasets of the required variables usually implies higher quality *ET* estimates.

References

Aires, F., and C. Prigent (2006), Toward a new generation of satellite surface products?, *Journal of Geophysical Research*, *111*.

Aires, F., C. Prigent, and W. B. Rossow (2005), Sensitivity of microwave and infrared satellite observations to soil moisture at a global scale. II: Global statistical relationships, *J. Geophys. Res.*, *110*.

Allen, R. G., L. S. Perista, D. Raes, and M. Smith (1998), Crop evapotranspiration - Guidelines for computing crop water requirements; FAO Irrigation and Drainage Papers - 56*Rep.*, FAO - Food and Agriculture Organization of the United Nations, Rome.

Anderson, M. C., W. P. Kustas, and J. M. Norman (2007), Upscaling Flux Observations from Local to Continental Scales Using Thermal Remote Sensing, *Agronomy Journal*, *99*(1), 240-254.

Anderson, M. C., J. M. Norman, G. R. Diak, W. P. Kustas, and J. R. Mecikalski (1997), A two-source time-integrated model for estimating surface fluxes using thermal infrared remote sensing, *Remote Sensing of Environment*, *60*(2), 195-216.

Anderson, M. C., et al. (2011), Mapping daily evapotranspiration at field to continental scales using geostationary and polar orbiting satellite imagery, *Hydrol. Earth Syst. Sci.*, *15*(1), 223-239.

Baldocchi, D., et al. (2001), FLUXNET: A New Tool to Study the Temporal and Spatial Variability of Ecosystem–Scale Carbon Dioxide, Water Vapor, and Energy Flux Densities, *Bulletin of the American Meteorological Society*, *82*(11), 2415-2434.

Barton, I. J. (1979), Parameterization of the evaporation from non-saturated surfaces, *Journal of Applied Meteorology*, *18*(1), 43-47.

Bastiaanssen, W. G. M., M. Menenti, R. A. Feddes, and A. A. M. Holtslag (1998), A remote sensing surface energy balance algorithm for land (SEBAL). 1. Formulation, *Journal of Hydrology*, *212-213*, 198-212.

Batra, N., S. Islam, V. Venturini, G. Bisht, and L. Jiang (2006), Estimation and comparison of evapotranspiration from MODIS and AVHRR sensors for clear sky days over the Southern Great Plains, *Remote Sens. Environ.*, *103*, 1-15.

Brenner, A. J., and L. D. Incoll (1997), The effect of clumping and stomatal response on evaporation from sparsely vegetated shrublands, *Agricultural and Forest Meteorology*, *84*(3–4), 187-205.

Calder, I. R. (1990), *Evaporation in the Uplands*, Wiley Chichester.

Carlson, T. N. (2007), An Overview of the "Triangle Method" for Estimating Surface Evapotranspiration and Soil Moisture from Satellite Imagery, *Sensors*, *7*(8), 1612-1629.

Carlson, T. N., and M. J. Buffum (1989), On estimating total daily evapotranspiration from remote surface temperature measurements, *Remote Sensing of Environment*, *29*(2), 197-207.

Carlson, T. N., E. M. Perry, and T. J. Schmugge (1990), Remote estimation of soil moisture availability and fractional vegetation cover for agricultural fields, *Agricultural and Forest Meteorology*, *52*(1-2), 45-69.

Carlson, T. N., W. J. Capehart, and R. R. Gillies (1995), A new look at the simplified method for remote sensing of daily evapotranspiration, *Remote Sensing of Environment*, *54*(2), 161-167.

Cleugh, H. A., R. Leuning, Q. Mu, and S. W. Running (2007), Regional evaporation estimates from flux tower and MODIS satellite data, *Remote Sensing of Environment*, *106*(3), 285-304.

Colaizzi, P. D., A. D. Schneider, S. R. Evett, and T. A. Howell (2004), Comparison of SDI, LEPA, and spray irrigation performance for grain sorghum, *Transactions of the ASAE*, *47*(5).

Courault, D., B. Seguin, and A. Olioso (2005), Review on estimation of evapotranspiration from remote sensing data: From empirical to numerical modeling approaches, *Irrigation and Drainage Systems*, *19*(3), 223-249.

Farahani, H. J., and L. R. Ahuja (1996), *Evapotranspiration modeling of partial canopy/residue-covered fields*, American Society of Agricultural Engineers, St. Joseph, MI, ETATS-UNIS.

Fisher, J. B., K. P. Tu, and D. D. Baldocchi (2008), Global estimates of the land-atmosphere water flux based on monthly AVHRR and ISLSCP-II data, validated at 16 FLUXNET sites, *Remote Sensing of Environment*, *112*(3), 901-919.

Friedl, M. A., D. Sulla-Menashe, B. Tan, A. Schneider, N. Ramankutty, A. Sibley, and X. Huang (2010), MODIS Collection 5 global land cover: Algorithm refinements and characterization of new datasets, *Remote Sensing of Environment*, *114*(1), 168-182.

Gash, J. H. (1979), An analytical model of rainfall interception by forests quarterly, *Journal of Royal Meteorological Society*, *105*, 43-45.

Gash, J. H. C., and J. B. Stewart (1977), The evaporation from Thetford Forest during 1975, *Journal of Hydrology*, *35*, 385-396.

Global Soil Data Task Group (2010), Global Gridded Surfaces of Selected Soil Characteristics, International Geosphere-Biosphere Programme – Data and Information System), Oak Ridge National Laboratory Distributed Active Archive Center, Oak Ridge, TE, at: http://www.daac.ornl.gov.

Goward, S. N., G. D. Cruickshanks, and A. S. Hope (1985), Observed relation between thermal emission and reflected spectral radiance of a complex vegetated landscape, *Remote Sensing of Environment*, *18*(2), 137-146.

Gutman, G. G. (1999), On the use of long-term global data of land reflectances and vegetation indices derived from the advanced very high resolution radiometer, *J. Geophys. Res.*, *104*, 6241-6255.

Hansen, M. C., J. R. G. Townshend, R. S. DeFries, and M. Carroll (2005), Estimation of tree cover using MODIS data at global, continental and regional/local scales, *International Journal of Remote Sensing*, *26*(19), 4359-4380.

Jackson, R. D., R. J. Reginato, and S. B. Idso (1977), Wheat canopy temperature: a practical tool for evaluating water requirements, *Water Resources Research*, *13*(3), 651-656.

Jia, L., Z. Su, B. van den Hurk, M. Menenti, A. Moene, H. A. R. De Bruin, J. J. B. Yrisarry, M. Ibanez, and A. Cuesta (2003), Estimation of sensible heat flux using the Surface Energy Balance System (SEBS) and ATSR measurements, *Physics and Chemistry of the Earth, Parts A/B/C*, *28*(1–3), 75-88.

Jiang, L., and S. Islam (2001), Estimation of surface evaporation map over Southern Great Plains using remote sensing data, *Water Resour. Res.*, *37*(2), 329-340.

Jiménez, C., C. Prigent, and F. Aires (2009), Toward an estimation of global land surface heat fluxes from multisatellite observations, *J. Geophys. Res*, *114*(D06305), D06305.

Jiménez, C., et al. (2011), Global intercomparison of 12 land surface heat flux estimates, J. Geophys. Res., 116, D02102, doi:10.1029/2010JD014545.

Joyce, R. J., J. E. Janowiak, P. A. Arkin, and P. Xie (2004), A method that produces global precipitation estimates from passive microwave and infrared data at high spatial and temporal resolution, *J. Hydrometeorol.*, *5*, 487-503.

Jung, M., M. Reichstein, and A. Bondeau (2009), Towards global empirical upscaling of FLUXNET eddy covariance observations: validation of a model tree ensemble approach using a biosphere model, *Biogeosciences*, *6*(10), 2001-2013.

Jung, M., M. Reichstein, P. Ciais, S. I. Seneviratne, J. Sheffield, M. L. Goulden, G. Bonan, A. Cescatti, J. Chen, and R. de Jeu (2010), Recent decline in the global land evapotranspiration trend due to limited moisture supply, *Nature*, *467*(7318), 951-954.

Jupp, D. L. B., G. Tian, T. R. McVicar, Y. Qin, and L. Fuqin (1998), Soil Moisture and Drought Monitoring Using Remote Sensing. I: Theoretical Background and Methods, *Canberra, CSIRO Earth Observation Centre*, *96*.

Kalma, J., T. McVicar, and M. McCabe (2008), Estimating Land Surface Evaporation: A Review of Methods Using Remotely Sensed Surface Temperature Data, *Surveys in Geophysics*, *29*(4), 421-469.

Kelly, R. E., A. T. Chang, L. Tsang, and J. L. Foster (2003), A prototype AMSR-E global snow area and snow depth algorithm, *Geoscience and Remote Sensing, IEEE Transactions on*, *41*(2), 230-242.

Kustas, W. P., and C. S. T. Daughtry (1990), Estimation of the soil heat flux/net radiation ratio from spectral data, *Agricultural and Forest Meteorology*, *49*(3), 205-223.

Kustas, W. P., and J. M. Norman (1999), Evaluation of soil and vegetation heat flux predictions using a simple two-source model with radiometric temperatures for partial canopy cover, *Agricultural and Forest Meteorology*, *94*(1), 13-29.

Leuning, R., Y. Q. Zhang, A. Rajaud, H. Cleugh, and K. Tu (2008), A simple surface conductance model to estimate regional evaporation using MODIS leaf area index and the Penman-Monteith equation, *Water Resour. Res.*, *44*(10), W10419.

Lhomme, J. P., C. Montes, F. Jacob, and L. Prévot (2012), Evaporation from Heterogeneous and Sparse Canopies: On the Formulations Related to Multi-Source Representations, *Boundary-Layer Meteorology*, *144*(2), 243-262.

Liu, Y. Y., R. A. M. de Jeu, M. F. McCabe, J. P. Evans, and A. I. J. M. van Dijk (2011), Global long-term passive microwave satellite-based retrievals of vegetation optical depth, *Geophys. Res. Lett.*, *38*(18), L18402.

Makkink, G. F. (1957), Testing the Penman formula by means of lysimeters, *Journal of the Institution of Water Engineers*, *11*, 277-288.

McCabe, M. F., and E. F. Wood (2006), Scale influences on the remote estimation of evapotranspiration using multiple satellite sensors, *Remote Sensing of Environment*, *105*(4), 271-285.

Menenti, M., and B. J. Choudhury (1993), Parameterization of land surface evaporation by means of location dependent potential evaporation and surface temperature range.

Miralles, D. G., M. van den Berg, R. Teuling, and R. A. M. De Jeu (2012), Soil moisture-temperature coupling: A multiscale observational analysis, *Geophysical Research Letters*(doi:10.1029/2012GL053703).

Miralles, D. G., J. H. Gash, T. R. H. Holmes, R. A. M. de Jeu, and A. Dolman (2010), Global canopy interception from satellite observations, *Journal of Geophysical Research*, *115*(D16), D16122.

Miralles, D. G., R. A. M. De Jeu, J. H. Gash, T. R. H. Holmes, and A. J. Dolman (2011a), Magnitude and variability of land evaporation and its components at the global scale, *Hydrol. Earth Syst. Sci.*, *15*(3), 967-981.

Miralles, D. G., T. R. H. Holmes, R. A. M. De Jeu, J. H. Gash, A. G. C. A. Meesters, and A. J. Dolman (2011b), Global land-surface evaporation estimated from satellite-based observations, *Hydrol. Earth Syst. Sci.*, *15*(2), 453-469.

Mueller, B., et al. (2011), Evaluation of global observations-based evapotranspiration datasets and IPCC AR4 simulations, Geophys. Res. Lett., 38, L06402, doi:10.1029/ 2010GL046230.

Monin, A. S., and A. M. Obukhov (1954), Basic laws of turbulent mixing in the ground layer of the atmosphere (in Russian), *Tr. Geofiz. Inst. Akad. Nauk SSSR*(151), 163-187.

Monteith, J. L. (1965), Evaporation and environment, *Symp. Soc. Exp. Biol.*, *19*, 205-234.

Mu, Q., M. Zhao, and S. W. Running (2011), Improvements to a MODIS global terrestrial evapotranspiration algorithm, *Remote Sensing of Environment*, *115*(8), 1781-1800.

Mu, Q., F. A. Heinsch, M. Zhao, and S. W. Running (2007), Development of a global evapotranspiration algorithm based on MODIS and global meteorology data, *Remote Sensing of Environment*, *111*(4), 519-536.

Murphy, D. M., and T. Koop (2005), Review of the vapour pressures of ice and supercooled water for atmospheric applications, *Quarterly Journal of the Royal Meteorological Society*, *131*(608), 1539-1565.

Nemani, R. R., and S. W. Running (1989), Estimation of Regional Surface Resistance to Evapotranspiration from NDVI and Thermal-IR AVHRR Data, *Journal of Applied Meteorology*, *28*(4), 276-284.

New, M., M. Hulme, and P. Jones (2000), Representing twentieth-century space-time climate variability. Part II: Development of 1901-96 monthly grids of terrestrial surface climate, *Journal of Climate*, *13*(13), 2217-2238.

Norman, J. M., W. P. Kustas, and K. S. Humes (1995), Source approach for estimating soil and vegetation energy fluxes in observations of directional radiometric surface temperature, *Agricultural and Forest Meteorology*, *77*(3-4), 263-293.

Owe, M., R. de Jeu, and T. Holmes (2008), Multisensor historical climatology of satellite-derived global land surface moisture, *Journal of Geophysical Research*, *113*(F1), F01002.

Penman, H. L. (1948), Natural Evaporation from Open Water, Bare Soil and Grass, *Proceedings of the Royal Society of London. Series A. Mathematical and Physical Sciences*, *193*(1032), 120-145.

Price, J. C. (1990), Using spatial context in satellite data to infer regional scale evapotranspiration, *Geoscience and Remote Sensing, IEEE Transactions on*, *28*(5), 940-948.

Priestley, C. H. B., and R. J. Taylor (1972), On the Assessment of Surface Heat Flux and Evaporation Using Large-Scale Parameters, *Monthly Weather Review*, *100*(2), 81-92.

Roerink, G. J., Z. Su, and M. Menenti (2000), S-SEBI: A simple remote sensing algorithm to estimate the surface energy balance, *Physics and Chemistry of the Earth, Part B: Hydrology, Oceans and Atmosphere*, *25*(2), 147-157.

Rudolf, B., and U. Schneider (2005), Calculation of gridded precipitation data for the global land-surface using in-situ gauge observations, paper presented at Proceedings of the 2nd workshop of the International Precipitation Working Group IPWG.

Schüttemeyer, D., C. Schillings, A. F. Moene, and H. A. R. de Bruin (2007), Satellite-based actual evapotranspiration over drying semiarid terrain in West Africa, *J. Appl. Meteor. Climatol.*, *46*, 97-111.

Seguin, B., and B. Itier (1983), Using midday surface temperature to estimate daily evaporation from satellite thermal IR data, *International Journal of Remote Sensing*, *4*(2), 371-383.

Seneviratne, S. I., D. Lüthi, M. Litschi, and C. Schär (2006), Land–atmosphere coupling and climate change in Europe, *Nature*, *443*(7108), 205-209.

Sheffield, J. (2008), Global Drought in the 20th and 21st Centuries - Analysis of retrospective simulations and future projections of soil moisture, xii+206 pp, Wageningen University.

Sheffield, J., and E. F. Wood (2007), Characteristics of global and regional drought, 1950–2000: Analysis of soil moisture data from off-line simulation of the terrestrial hydrologic cycle, *Journal of Geophysical Research*, *112*(D17), D17115.

Sheffield, J., G. Goteti, and E. F. Wood (2006), Development of a 50-year high-resolution global dataset of meteorological forcings for land surface modeling, *Journal of Climate*, *19*(13), 3088-3111.

Sheffield, J., E. F. Wood, and F. Munoz-Arriola (2010), Long-term regional estimates of evapotranspiration for Mexico based on downscaled ISCCP data, *Journal of Hydrometeorology*, *11*(2), 253-275.

Shuttleworth, W. J., and J. S. Wallace (1985), Evaporation from sparse crops-an energy combination theory, *Quarterly Journal of the Royal Meteorological Society*, *111*(469), 839-855.

Sobrino, J. A., M. Gomez, J. C. Jiménez-Muñóz, and A. Olioso (2007), Application of a simple algorithm to estimate daily evapotranspiration from NOAA-AVHRR images for the Iberian Peninsula, *Remote Sens. Environ.*, *110*, 139-148.

Stackhouse, P. W., S. K. Gupta, S. J. Cox, J. C. Mikovitz, T. Zhang, and M. Chiacchio (2004), 12 year surface radiation budget data set, *GEWEX News*, *2004*(14).

Su, H., M. F. McCabe, E. F. Wood, Z. Su, and J. H. Prueger (2005), Modeling Evapotranspiration during SMACEX: Comparing Two Approaches for Local- and Regional-Scale Prediction, *Journal of Hydrometeorology*, *6*(6), 910-922.

Su, Z., W. Dorigo, D. Fernández-Prieto, M. Van Helvoirt, K. Hungershoefer, R. De Jeu, R. Parinussa, J. Timmermans, R. Roebeling, and M. Schröder (2010), Earth observation Water Cycle Multi-Mission Observation Strategy (WACMOS), *Hydrol. Earth Syst. Sci. Discuss*, *7*, 7899-7956.

Su, Z. B. (2002), A Surface Energy Balance System (SEBS) for estimation of turbulent heat fluxes from point to continental scale, paper presented at Spectra Workshop.

Tang, R. L., Z. L. Li, and B. H. Tang (2010), An application of the Ts-VI triangle method with enhanced edges determination for evapotranspiration estimation from MODIS data in arid and semi-arid regions: implementation and validation, *Remote Sens. Environ.*, *114*, 540–551.

Tittebrand, A., A. Schwieben, and F. Berger (2005), The influence of land surface parameters on energy flux densities derived from remote sensing data, *Meteorol. Z.*, *14*, 227–236.

Tucker, C. J., J. E. Pinzon, M. E. Brown, D. A. Slayback, E. W. Pak, R. Mahoney, E. F. Vermote, and N. El Saleous (2005), An extended AVHRR 8-km NDVI dataset compatible with MODIS and SPOT vegetation NDVI data, *International Journal of Remote Sensing*, *26*(20), 4485-4498.

Valente, F., J. David, and J. Gash (1997), Modelling interception loss for two sparse eucalypt and pine forests in central Portugal using reformulated Rutter and Gash analytical models, *Journal of Hydrology*, *190*(1), 141-162.

Venturini, V., S. Islam, and L. Rodriguez (2008), Estimation of evaporative fraction and evapotranspiration from MODIS products using a complementary based model, *Remote Sensing of Environment*, *112*(1), 132-141.

Venturini, V., L. Rodriguez, and G. Bisht (2011), A comparison among different modified Priestley and Taylor equations to calculate actual evapotranspiration with MODIS data, *International Journal of Remote Sensing*, *32*(5), 1319-1338.

Vinukollu, R. K., E. F. Wood, C. R. Ferguson, and J. B. Fisher (2011), Global estimates of evapotranspiration for climate studies using multi-sensor remote sensing data: Evaluation of three process-based approaches, *Remote Sensing of Environment*, *115*(3), 801-823.

Wang, K., and S. Liang (2008), An improved method for estimating global evapotranspiration based on satellite determination of surface net radiation, vegetation index, temperature, and soil moisture, paper presented at Geoscience and Remote Sensing Symposium, 2008. IGARSS 2008. IEEE International, IEEE.

Wang, K., and R. E. Dickinson (2012), A review of global terrestrial evapotranspiration: Observation, modeling, climatology, and climatic variability, *Rev. Geophys.*, *50*(2), RG2005.

Wang, K., R. E. Dickinson, M. Wild, and S. Liang (2010a), Evidence for Decadal Variation in Global Terrestrial Evapotranspiration between 1982 and 2002, Part 1: Model Development, *J. Geophys. Res.*, *115*.

Wang, K., R. E. Dickinson, M. L. Wild, and S. Liang (2010b), Evidence for Decadal Variation in Global Terrestrial Evapotranspiration between 1982 and 2002, Part 2: Results, *J. Geophys. Res.*, *115*.

Zhang, Y., W. B. Rossow, A. A. Lacis, V. Oinas, and M. I. Mishchenko (2004), Calculation of radiative fluxes from the surface to top of atmosphere based on ISCCP and other global data sets: Refinements of the radiative transfer model and the input data, *Journal of Geophysical Research*, *109*(D19).

Zhang, K., J. S. Kimball, R. R. Nemani, and S. W. Running (2010a), A continuous satellite□derived global record of land surface evapotranspiration from 1983 to 2006, Water Resour. Res., 46, W09522, doi:10.1029/2009WR008800.

Zhang, Y., R. Leuning, L. B. Hutley, J. Beringer, I. McHugh, and J. P. Walker (2010b), Using long-term water balances to parameterize surface conductances and calculate evaporation at 0.05 spatial resolution, *Water Resources Research*, *46*(5), W05512.

Zhang, Y., R. Leuning, F. H. S. Chiew, E. Wang, L. Zhang, C. Liu, F. Sun, M. C. Peel, Y. Shen, M. Jung, (2012), Decadal Trends in Evaporation from Global Energy and Water Balances. *J. Hydrometeor*, 13, 379–391, doi: http://dx.doi.org/10.1175/JHM-D-11-012.1

Zhang, Y. Q., F. H. S. Chiew, L. Zhang, R. Leuning, and H. A. Cleugh (2008), Estimating catchment evaporation and runoff using MODIS leaf area index and the Penman-Monteith equation, *Water Resour. Res.*, *44*(10), W10420.

Zhao, M., F. A. Heinsch, R. R. Nemani, and S. W. Running (2005), Improvements of the MODIS terrestrial gross and net primary production global data set, *Remote sensing of Environment*, *95*(2), 164-176.